A New Method for Searching the Enrichment Element in Extended Finite Element Method

Xiaofang Jiang, Zhenghong Huang, Rui Luo, Hong Zuo, Xing Zheng, and Shouchun Deng*

Abstract—**Considering the characteristics of the structured mesh in the extended finite element method (XFEM), a new method is proposed to accurately search the enrichment element, which can determine enrichment type and simultaneously obtain the intersection position between the crack and the element boundary. Importantly, this intersection position information can guarantee accuracy when calculating the discontinuity element's stiffness matrix. In the new method, considering only the nodes of the enrichment elements, computation speed is increased and storage consumption is lower than that of the level set method (LSM). Numerical simulations were used to verify the advantages of the proposed method over the LSM for higher algorithm accuracy, higher computing efficiency, and lower storage consumption, and to explore the potential for efficient computing in three-dimensional (3D) situations. In addition, the feasibility of using the new method for efficient computation in 3D cases was verified.**

Index Terms—**XFEM, Structured mesh, Element boundary, Intersection information, Level set method (LSM)**

I. Introduction

In many engineering projects, catastrophic accidents are the result of fracture failure. In geotechnical engineering, rock masses often contain a discontinuous surface that can develop continuously under geostress, blasting, or hydrostatic loads, which can lead to discontinuous face interpenetrating (perforating) and cause instability. Conversely, in shale gas exploitation, water pressure is exerted on the perforation cracks and primary fractures to drive the crack growth. With better driving of the fractured network, the shale gas yield increases. Therefore, the propagation of the crack and prediction of the crack growth are critical to engineering practice. At present, there are many numerical methods to process discontinuity problems, such as the finite element method (FEM) [1], boundary element method (BEM) [4], discrete element method (DEM) [5], meshless method [6], and extended finite element method (XFEM) [7]. Belytschko and Black [7] proposed XFEM in a standard FE framework without re-meshing to address drawbacks in simulating discontinuity problems. Because of the characterizations and advantages of XFEM for discontinuity problems, it can be developed rapidly and has been widely employed to solve a variety of problems, such as simulating inclusions and holes [10], frictional contact [11], crack growth [14], fluid-structure coupling [20], multifluid flows [24], hydraulic fracturing [23], and several other discontinuity problems.

To further developthe finite element method in crack growth, Moës et al. [31] introduced the Heaviside function and the asymptotic crack tip displacement field function as enrichment shape functions to describe the displacement field's discontinuity of those elements, including the crack surface and tip, respectively. The nodes of the crack-crossed element and crack tip-embedded element are enriched by the Heaviside function and the asymptotic function respectively.

Osher and Sethian [32] devised the level set method (LSM) to trace the motion of an interface in two or three dimensions, and the method was used to find the crack-embedded element [15]. The LSM can be used to describe cracks, or interfaces between different materials, and to model their shapes [33]. As a powerful numerical method for interface tracking, the LSM has played an important role in digital image processing and in motion interface tracking in the XFEM. The key idea of the LSM for capturing discontinuous interfaces is to replace the real interface with a zero level set function $\phi\left(x(t),t\right)$ [34]. Thus, the level set value of node X can be obtained by the sign distance function in XFEM [10]. To accurately capture the location of the crack, two LS functions are needed [17]: (a) the crack LS function ϕ, which is orthogonal to (b) the LS function ψ at the crack tip. The type of the element can then be determined based on the two LS values of the element nodes.

When the method is embedded into higher dimensions and applied to the entire grid, it is inefficient [38]. For the sake of computational efficiency, Adalsteinsson and Sethian [39] introduced the narrow-band LS method in which only the nodes in the narrow band are used to calculate the values of the LS. Sethian [40] introduced the fast-marching method, which was directed by an extreme one-cell version of the narrow-band approach. Nodes are classified as accepted, tentative, and distant nodes by solving an Eikonal equation,

Manuscript received October 24, 2019; first revised April 02, 2020; second revised June 05, 2020. This study was supported by the Strategic Program of Chinese Academy of Sciences (Shale fracturing and multi-scale seepage in shale reservoir, Grant No. XDB10030400) and the Hundred Talent Program of Chinese Academy of Sciences (Shale hydraulic fracturing and multi-scale seepage mechanism and model, Grant No. Y323081C01).

Xiaofang Jiang, Rui Luo, Hong Zuo, and Xing Zheng are with State Key Laboratory of Geomechanics and Geotechnical Engineering, Institute of Rock and Soil Mechanics, Chinese Academy of Sciences, Wuhan, Hubei 430071, China and University of Chinese Academy of Sciences, Beijing, 100049, China (e-mail: jiangxiaofang@whu.edu.cn, 419499451@qq.com, hzuo@mail.whrsm.ac.cn, and 992551961@qq.com).

Zhenghong Huang, PhD, graduated from State Key Laboratory of Geomechanics and Geotechnical Engineering, Institute of Rock and Soil Mechanics, Chinese Academy of Sciences, Wuhan, Hubei 430071, China and University of Chinese Academy of Sciences, Beijing, 100049, China, now works for the First Construction Engineering Limited Company of China Construction Third Engineering Bureau, Wuhan, Hubei 430040, China (e-mail: huangzhenghong14@mails.ucas.ac.cn).

Shouchun Deng*, corresponding author, is a professor in State Key Laboratory of Geomechanics and Geotechnical Engineering, Institute of Rock and Soil Mechanics, Chinese Academy of Sciences, Wuhan 430071, China (e-mail: scdeng@whrsm.ac.cn).

which is the concept behind the fast-marching method [41]. Only the set of accepted nodes is needed to calculate the values of the LS, and the judgment is the same as using the LSM to determine the type [18]. Sethian [34] improved the fast-marching method and Chopp [44] used it to trace the geometric position of a discontinuous interface in the XFEM [45]. Ventura et al. [14] proposed a vector LSM in the XFEM to describe the location and propagation of cracks, but this method is seldom used in practical applications.

Even though the LS and fast-marching methods can capture the position of the crack, the intersection information between the crack and element boundary, as well as the inflection point of the crack, cannot be obtained. Nevertheless, this information is useful when subdividing the elements [31], integrating the contact surface in the contact problem [38], and dispersing the fluid in the crack network [21]. These algorithms are based on nodes without considering the relationship between the element boundary and crack; additionally, the type of the crack-tip-embedded element may not be judged correctly.

A key problem in the XFEM is the inability to search for the enrichment element and then to determine the type of enrichment element. The elements should be classified as standard, crack-crossed, and crack tip-embedded elements, as well as a blending element that contains standard and enriched nodes in the calculation. The LS and fast-marching methods play an important role in the XFEM by determining the relative position between the crack and element; however, they fail to capture information about the intersection of the crack and element boundary. This information is vital when subdividing the enrichment element. Actually, the use of the LSM in the XFEM is not necessary or mandatory [17]. On the basis of the position relationships between the structured mesh element and the crack, a method for searching the enrichment element and obtaining the intersection information that can be used to guarantee the accuracy of the stiffness matrix of enriched discontinuity element is proposed in this paper. The method not only avoids the misjudgment of the crack-tip-embedded element, but also contributes to the efficiency of the calculation because one needs to compute only the signed distance value of the enrichment node.

The remainder of this paper is organized as follows. Section II presents the governing equations and framework of the XFEM. Section III presents the different searching methods. Section IV gives the method for the element integral and Section V provides numerical examples. Finally, Section VI provides conclusions.

II. Governing Equations and XFEM Framework

A. Governing Equations

The linear elasticity small deformation governing equations in two-dimensional (2D) problems can be found in references [31]; they are described here briefly. Ω is the elastic body and Γ is the boundary of the domain, where the boundary Γ is composed of arbitrary cracks Γ_c^i, displaced boundary Γ_u^i, and the force boundary Γ_f^i. Then, prescribed tractions $\bar{f}$ and displacements $\bar{u}$ are imposed on the boundaries Γ_f and Γ_u, respectively, as shown in Fig. 1.

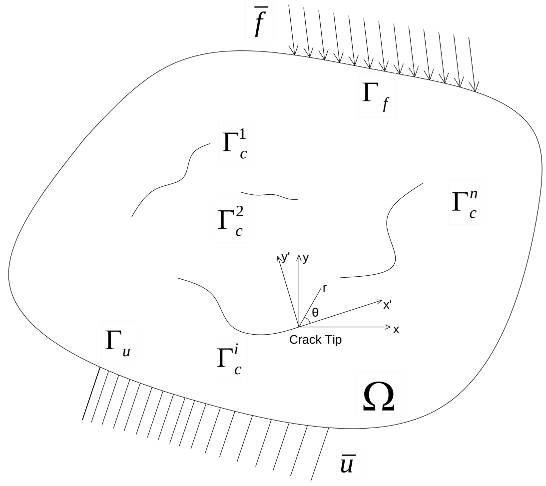

Fig. 1. The domain contains different boundaries.

According to the equilibrium equation in elastic mechanics, the related equations can be given by

$$\nabla\sigma_{ij,j} + b_i = 0 \text{ in } \Omega \tag{1}$$

$$u = \bar{u} \text{ on } \Gamma_u \tag{2}$$

$$\sigma \cdot n = \bar{f} \text{ on } \Gamma_f \tag{3}$$

$$\sigma \cdot n = 0 \text{ on } \Gamma_c \tag{4}$$

where $\sigma_{ij,j}$ is the matrix of stress tensor; b_j is the body force per unit volume of the domain; Γ_f, Γ_u, and Γ_c are the boundaries of force, displacement, and cracks, respectively; and n is the normal vector of the boundary.

In addition, the relationship between stress and strain is

$$\sigma = C : \varepsilon \tag{5}$$

$$\varepsilon = \nabla_s u \tag{6}$$

where C is the elasticity tensor, and ε and ∇_s are the strain tensor and symmetric gradient operator, respectively.

B. XFEM Framework

Equation (7) is based on partition unity and was first proposed by Belytschko and Black [6]; the enrichment shape function was introduced by Moës [31]. The method without re-meshing is called the XFEM:

$$\begin{aligned} u^h(x) = &\sum_{i\in s} N_i(x) u_i^S + \sum_{i_c}^{N_c} \sum_{j\in s_H} N_j(x)\phi(x) u_{ji_c} \\ &+ \sum_{k\in s_T} N_k(x)\varphi(x) u_k \end{aligned} \tag{7}$$

where $\phi(x)$ and $\varphi(x)$ are the enrichments, u^h is the displacement field of the nodes, u^S is the standard displacement of node x, u_j and u_k are the displacement fields of enriched node x, S is the set of all nodes, S_H and S_T are the sets of enriched nodes.

With this development, the final equation can be written as (8) [49]:

$$\begin{aligned} u^h(x) = &\sum_{i\in s} N_i(x) u_i^S \\ &+ \sum_{i_c}^{N_c} \sum_{j\in s_H} N_j(x)\left(H^{i_c}(x) - H^{i_c}(\mathrm{x}_j)\right) u_{j\ i_c}^H \\ &+ \sum_{k\in s_T} N_k(x)\left(\mathrm{B}(x) - \mathrm{B}(\mathrm{x}_k)\right) u_k^T \end{aligned} \tag{8}$$

where u^H and S_H are the displacements of node x enriched by the Heaviside step function and asymptotical function, respectively, and S_H and S_T are the respective sets of nodes enriched by the Heaviside step function and asymptotical function.

$H(x)$ is the Heaviside step function:

$$H(x)=\begin{cases}-1 & \text{for } x>0\\ 1 & \text{for } x<0\end{cases} \tag{9}$$

$\mathrm{B}(x)$ is the tip asymptotical function

$$\mathrm{B}(x)=\left[\sqrt{r}\sin\left(\frac{\theta}{2}\right)\quad \sqrt{r}\cos\left(\frac{\theta}{2}\right)\quad \sqrt{r}\sin\left(\frac{\theta}{2}\right)\sin(\theta)\quad \sqrt{r}\sin(\theta)\cos\left(\frac{\theta}{2}\right)\right] \tag{10}$$

where $\sqrt{r}$ and θ are polar coordinate parameters in the local crack-tip coordinate system.

III. Different Searching Methods

A. *LS Method*

The LSM was originally proposed to track the moving interface, which is composed of pixels in digital images. Later, this method was used to describe the crack interface and the search enrichment element in the XFEM. Element computation, particularly the enrichment element, is a key part of the XFEM, and only when the node is combined with the element does the calculation make sense. Because the LSM captures the crack location and determines that the enrichment element is based on the node, the intersection information between the crack and element cannot be obtained, and errors in judgment about the type of enrichment often occur in the calculation process.

To obtain the enrichment element, two LS functions [17] are needed to describe the position of the crack, as shown in Fig. 2.

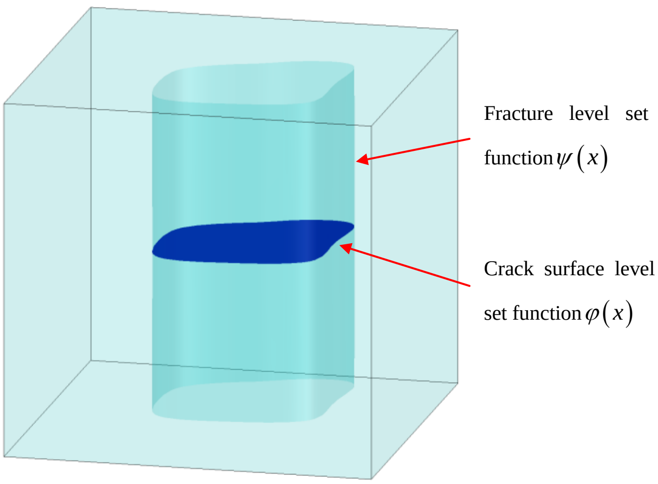

(a)

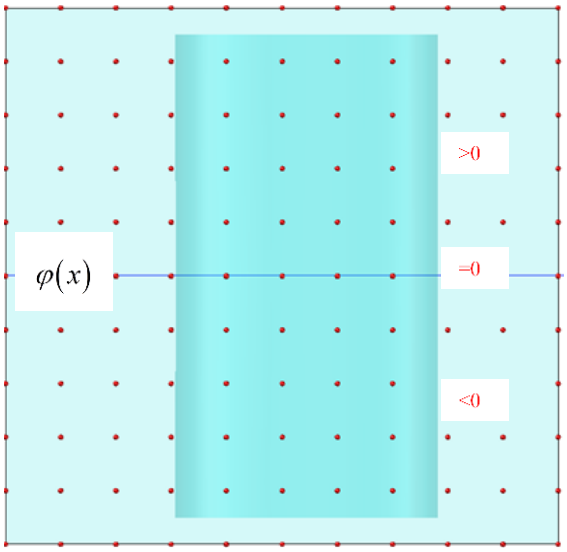

(b)

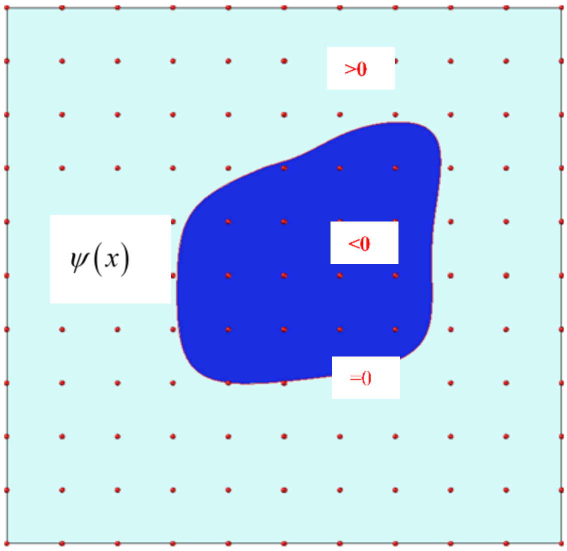

(c)

Fig. 2. (a) Two LS functions to describe the position for the crack; (b) crack surface LS function $\varphi(x)$ (front view); (c) fracture LS function $\psi(x)$ (top view).

From this figure, the two LS values of node x were defined as follows:

$$\varphi(x)=\begin{cases}>0 & \text{the node is above the crack surface}\\ 0 & \text{the node is on the crack surface}\\ <0 & \text{the node is down the crack surface}\end{cases} \tag{11}$$

$$\psi(x)=\begin{cases}>0 & \text{the node is outside the fracture}\\ 0 & \text{the node is on the fracture}\\ <0 & \text{the node is in the fracture}\end{cases} \tag{12}$$

A 2D crack model was considered as an example to evaluate the element type, as shown in Fig. 3.

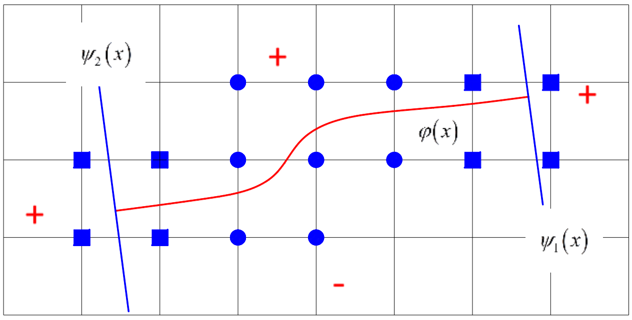

Fig. 3. Crack model for enrichment element in 2D model.

The enrichment elements and types of elements were determined using the following judgment method:

(a) If $\psi_{\min}(x) \bullet \psi_{\max}(x) < 0$ and $\varphi_{\min}(x) \bullet \varphi_{\max}(x) < 0$, then the element is a crack-tip-embedded element.

(b) If $\psi_{\max}(x) < 0$ and $\varphi_{\min}(x) \bullet \varphi_{\max}(x) < 0$, then the element is a crack-crossed element.

(c.1) If $\psi_{\max}(x) < 0$ and $\varphi_{\max}(x) < 0$, then the element is a standard element.

(c.2) If $\psi_{\max}(x) < 0$ and $\varphi_{\min}(x) > 0$, then the element is a standard element.

(c.3) If $\psi_{\min}(x) > 0$, then the element is the standard.

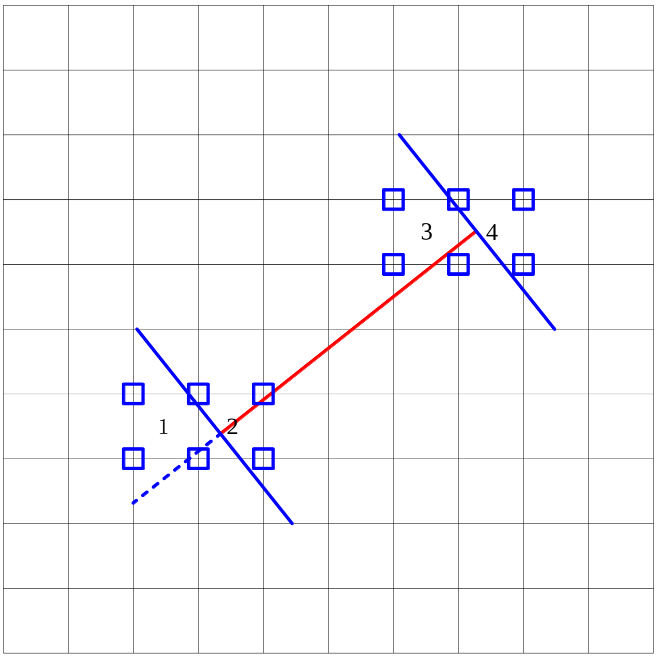

Fig. 4. Element types are judged incorrectly by the LS method.

From Fig. 4, it can be seen that elements 2 and 4 are crack-tip-embedded elements, element 1 is a standard element, and element 3 is a crack-crossed element, but elements 1 and 3 are incorrectly judged to be crack-tip-embedded elements by the LSM.

B. Proposed Method

The method proposed in this paper searches the enrichment element and determines the type of element based on the relative position between the element and the crack—that is, the intersection and disjoint. At the same time, this method captures the intersection information between the crack and element boundary. According to the enrichment element, one can calculate the signed distance value of the enrichment node used by the Heaviside function.

2D Algorithm

In the 2D model, because the crack is a 1D line, one can judge the type of enrichment element based on the relationship between the element boundary position and line position. Moreover, one can also obtain the intersection information in the calculation procedure.

It was assumed that the crack is presented by the function $f(x, y) = 0$, and the domain of the crack is restricted to the interval Ω, which is composed of monotony sub-intervals $\Omega_i = [p_i, p_{i+1}]$, as shown in Fig. 5.

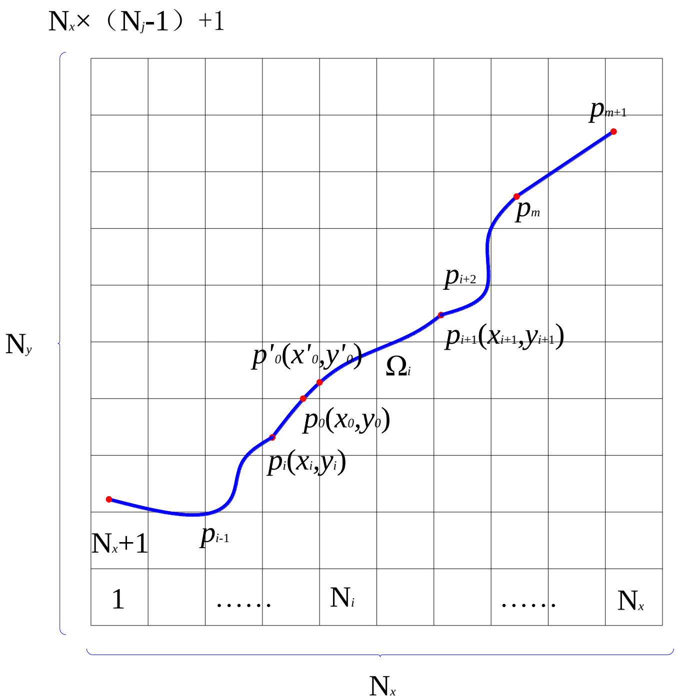

Fig. 5. Calculation model in two dimensions.

The number of the element embedded by the end point was obtained using the following equations:

$$Element\_Number = (N_j - 1) \times N_x + N_i \tag{13}$$

$$x \in \left[(N_i - 1) \times ELx, N_i \times ELx\right] \tag{14}$$

$$y \in \left[(N_j - 1) \times ELy, N_j \times ELy\right] \tag{15}$$

where *Element_Number* is the element number, N_x is the total number of elements in the x direction, N_i is the N_i^{th} element in the x direction, N_j is the N_j^{th} element in the y direction, ELx is the element length in the x direction, ELy is the element length in the y direction, and (x, y) is the arbitrary point in the plane.

The element is crossed by the crack, and one can calculate the intersection information between the crack and element boundary by the following equations:

$$x_0 = N_x \times ELx \in [x_i, x_{i+1}] \tag{16}$$

$$y_0 = f(x_0), \text{ and} \tag{17}$$

$$y_0 \in (y_i, y_{i+1}]; \text{ or} \tag{18}$$

$$y_0^{'} = N_y \times ELy \in (y_i, y_{i+1}] \tag{19}$$

$$x_0^{'} = f\left(y_0^{'}\right), \text{ and} \tag{20}$$

$$x_0^{'} \in \left(x_i, x_{i+1}\right] \tag{21}$$

where (x_0, y_0) or $(x_0^{'}, y_0^{'})$ is the intersection point between the crack and element boundary, and (x_i, y_i) and (x_{i+1}, y_{i+1}) are the end points of the interval Ω_i.

In the calculation, the enrichment elements and their type can be obtained only by the intersection point between the crack and element boundary, and by the end point of the interval Ω_i.

In MATLAB, the code can be implemented as follows:

- For the crack-tip-embedded element:

```
for Ni=1:Nx-1
 for Nj=1:Ny-1
  if judging the coordinate of crack tip 1 by equations (14) and (15)
      calculating the number of elements by equation (13)
  elseif judging the coordinate of crack tip 2 by equations (14) and (15)
          calculating the number of elements by equation (13)
  end
 end
end
```

- For the crack-crossed element

```
for i_interval = 1:length(CRACK(:,1))-1
   Cx = [CRACK(i_interval,1) CRACK(i_interval +1,1)];
   Cy = [CRACK(i_interval,2) CRACK(i_interval +1,2)];
   for Ni=1:Nx-1
     if judging the element boundary by equation (16)
       solving y0 by equation (17)
       if judging y0 by equation (18)
         for Nj=1:Ny-1
           if calculating Nj
             calculating the number of elements by equation (13)
           end
         end
       end
     end
   end
   for Nj=1:Ny-1
     if judging the element boundary by equation (19)
       solving x0 by equation (20)
       if judging x0 by equation (21)
         for Ni=1:Nx-1
         if calculate Ni
           calculating the number of elements by equation (13)
           end
          end
         end
        end
       end
      end
```

After updating crack growth in the 2D model, the algorithm for crack segment $m+1$ is the same as that for the crack segment i ($1 \leqslant i \leqslant m$). Additionally, only the crack segment $p_m p_{m+1}$ and the crack tip point p_{m+1} must be considered.

Signed Distance Value

According to (8), the nodes of the crack-crossed element are enriched by the Heaviside function, so one must determine the sign of the enrichment nodes. The signed distance value of the enrichment node was calculated using the following functions [10]:

$$\xi_i(\mathrm{x}) = \left\|\mathrm{x}_i - \mathrm{x}_{\min}\right\| sign\left[\mathrm{n}_{\min} \cdot \left(\mathrm{x}_i - \mathrm{x}_{\min}\right)\right] \tag{22}$$

$$\left\|\mathrm{x}_i - \mathrm{x}_{\min}\right\| = \min_{\substack{\mathrm{x}_j \in \Gamma_j \\ j=1,2\ldots,m}} \left\|\mathrm{x}_i - \mathrm{x}_j\right\| \tag{23}$$

where $\mathrm{x}_{\min}$ is the orthogonal projection of x on the interface, $\mathrm{n}_{\min}$ is its associated outward normal to the interface at $\mathrm{x}_{\min}$, and the interface $\Gamma\left(\Gamma = \bigcup_i^m \Gamma_i\right)$ consists of m segments Γ_i ($\Gamma_i = \left[\mathrm{x}_i, \mathrm{x}_{i+1}\right]$).

The calculation flowchart for the LSM and algorithm used in this paper are shown in Fig. 6. In the LSM, many variables are needed to store the data, such as the two LS values for all nodes and the temporary variables for the product of the minimum and maximum of the two LS values in an element for all elements. However, with the proposed method, the sign distance values must be stored only for the enriched nodes.

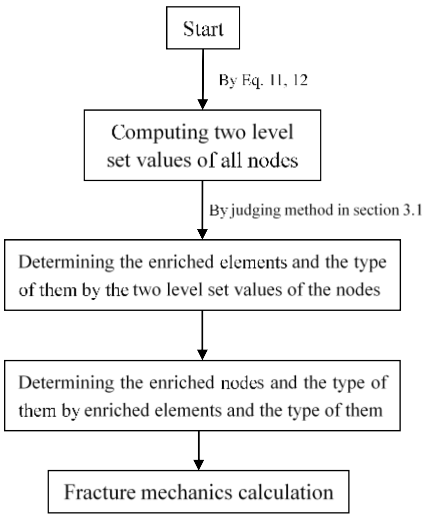

(a) Level set method (LSM).

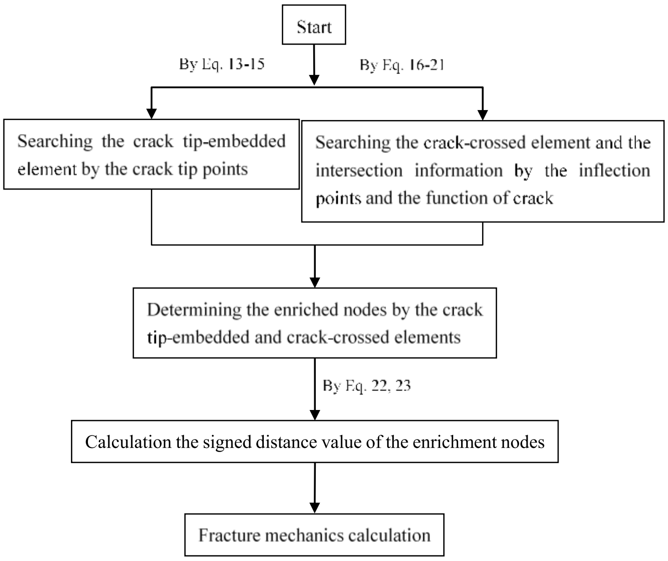

(b) Proposed method.
Fig. 6. Calculation flowchart in 2D model.

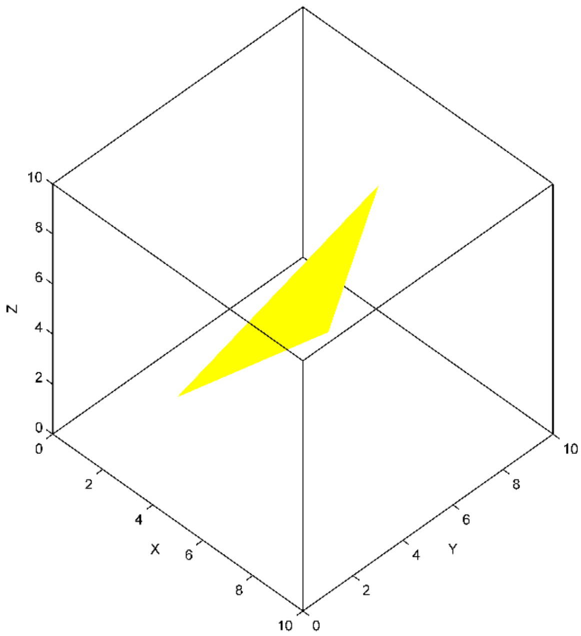

(a) Model containing a crack in the center.

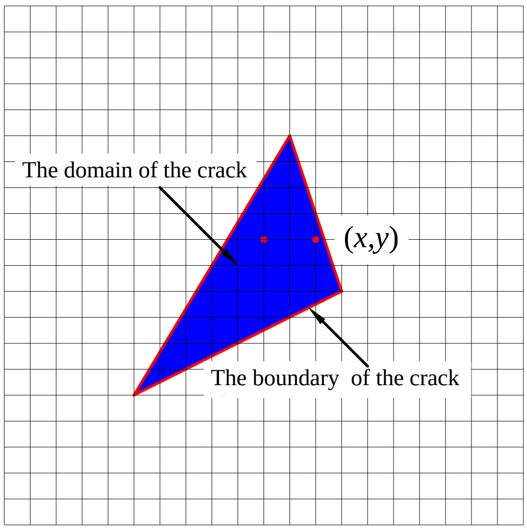

(b) Projection area and boundary of the crack in the z direction.
Fig. 7. Method in 3D model.

C. 3D Algorithm

In the 3D model, the crack is 2D, so the relationship between the boundaries of the crack and element should be considered. To simplify the algorithm, the projection equations were constructed and solved in three axis directions. The 2D algorithm is a special case of the projection algorithm in the xy-plane direction. Taking the xy-plane projection as an example, the following steps were taken.

Step 1: Compute the projection area and boundary of the crack, as shown in Fig. 7.

Step 2: Consider whether the arbitrary projection point (x, y) is in the area of the crack surface projection.

Step 3: According to the projection, use the coordinates (x, y) and crack function $f(x, y, z) = 0$ to obtain the coordinate values z, and then use the following equations to calculate the point in which element:

$$Element\_Number = N_x \times N_y \times N_k + (N_j - 1) \times N_x + N_i \quad (24)$$

$$x \in \left[(N_i - 1) \times ELx, N_i \times ELx \right] \quad (25)$$

$$y \in \left[(N_j - 1) \times ELy, N_j \times ELy \right] \quad (26)$$

$$z \in \left[(N_k - 1) \times ELz, N_k \times ELz \right] \quad (27)$$

where N_y is the total number of elements in the *y* direction, N_k is the $N_k{}^{th}$ element in the *z* direction, and *ELz* is the element length in the *z* direction.

Step 4: Determine the key point information of the intersection (x_0, y_0, z_0) between the element and crack by the projection point (x_0, y_0) in the projection crack plane, where

$$x_0 = N_x \times ELx \quad (28)$$

$$y_0 = N_y \times ELy \quad (29)$$

$$z_0 = f(x_0, y_0) \quad (30)$$

The other two projection directions are the same as that in the *xy*-plane direction.

IV. Element Integral

To obtain the stiffness matrix of the element, it is necessary to evaluate the integral of the stiffness matrix. The integral domain of the standard and blending elements is continuous, so it was possible to guarantee the accuracy of the calculation for the stiffness matrix of the element by selecting the appropriate Gaussian integral point. Accuracy of the enrichment stiffness matrix could not be guaranteed, however, because of the discontinuity of the enrichment element domain. Belytschko [50] suggested that the elements cut by discontinuities should be subdivided into sub-elements. The subdivision will be easy if the intersection points between the crack and element boundary and inflection points of the crack are known. Fig. 8(a) shows that five of the enrichment elements in the 2D model are embedded by two segment cracks, which are subdivided into sub-elements by the *delaunay* function in MATLAB, as shown in Fig. 8(b). The blue boxes (■) represent the intersection points between the crack and the element boundary, and the red circles (●)

represent the inflection points of the crack.

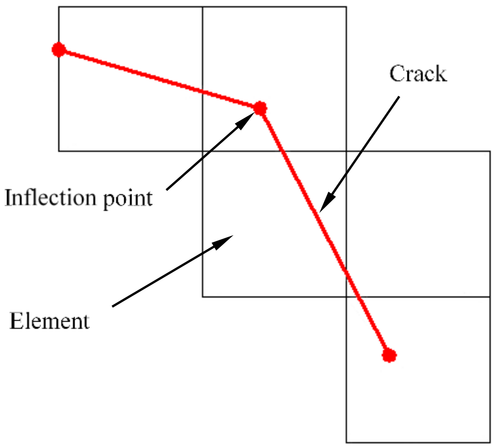

(a) Element embedded by crack.

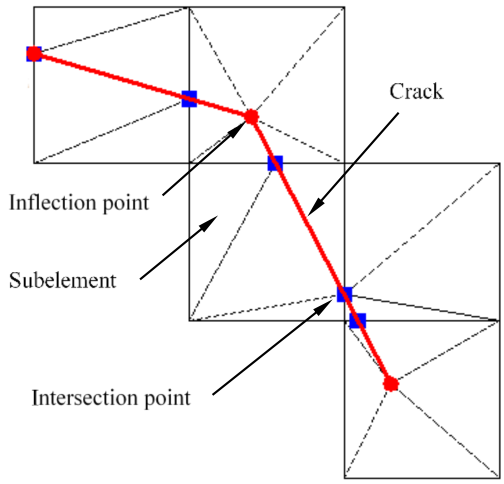

(b) Subdividing element by inflection and intersection points.
Fig. 8. Subdividing enriched element by *delaunay* function in MATLAB.

The stiffness matrix of the enrichment element can then be computed by the following equation

$$\begin{aligned} K^{enrich} &= \int_{\Omega} (B^{enrich})^{\mathrm{T}} D B^{enrich} d\Omega \\ &= \sum_{i=1}^{n} \int_{\Omega_i^{sub}} (B^{enrich})^{\mathrm{T}} D B^{enrich} d\Omega_i^{sub} \end{aligned} \tag{31}$$

where K^{enrich} is the stiffness matrix of the enrichment element, B^{enrich} is the strain-displacement matrix of the enrichment element, D is the constitutive matrix, and Ω is the domain of the enrichment element, which is composed of the sub-domain Ω_i^{sub}.

V. Numerical Examples

A. Illustration of Accuracy of Sub-Element Integral

To illustrate the accuracy of the enriched discontinuous element stiffness matrix, the stress intensity factors (SIFs) for a plate with an angled center crack were calculated, and uniform tension stress was applied on the lower and upper edges of the plate, as shown in Fig. 9.

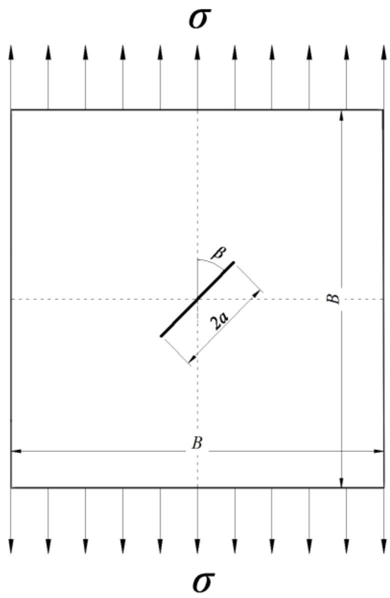

Fig. 9. Plate with center crack at angle β.

The non-dimensional size of the model is given as follows: $a/B = 0.1373$. The numerical solutions were compared with the sub-elements method and rectangular sub-grids method [43] with the exact SIF [51], which are given as follows:

$$K_{\mathrm{I}} = \sigma\sqrt{\pi a}\sin^2\beta \tag{32}$$

$$K_{\mathrm{II}} = \sigma\sqrt{\pi a}\sin\beta\cos\beta \tag{33}$$

The results in Fig. 10 show the solution and sub-element's excellent agreement with the exact solution for the entire range of β, but the solution obtained using the rectangular sub-grids method does not agree.

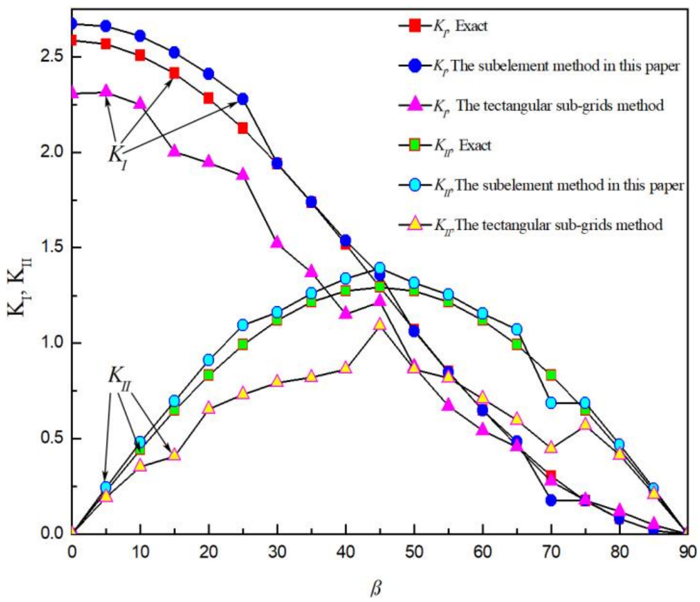

Fig. 10. Relationship between stress intensity factor and angle.

B. Computing for Center Slant Crack

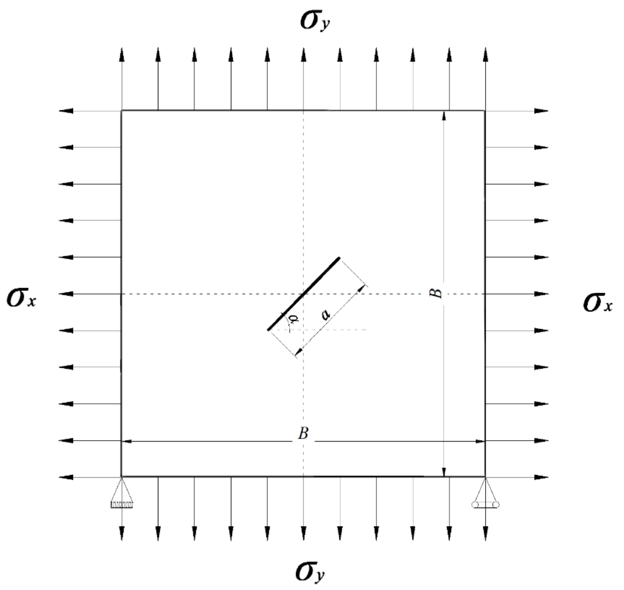

Fig. 11. Plate with center slant crack.

Fig. 11 shows a center slant crack in the plate. The non-dimensional size of the model is given as follows: $a/B = 0.2838$, $\beta = 45.21^{\circ}$, $\sigma_x/\sigma_y = 2.5$, and $\Delta a/B = 0.03226$, where Δa is the step length and the mesh number is 31 × 31. This example is used to discuss the accuracy of searching the enrichment elements, and to compare overall computation times using the LSM and the proposed method. The maximum circumferential stress criterion [52] will be used to compute the direction of crack growth [7]:

$$\theta = 2\arctan\left(\frac{1}{4}\left(\frac{K_I}{K_{II}} \pm \sqrt{\left(\frac{K_I}{K_{II}}\right)^2 + 8}\right)\right) \tag{34}$$

where θ is the angle for crack propagation in the local coordinate system, and K_I and K_{II} are the SIFs of modes I and II, respectively.

Searching Enrichment Elements

The LSM may sometimes misjudge some of the enrichment elements for a slant crack. The different types of enriched nodes in the first and third steps are shown in Fig. 12, and the nodes enclosed by a red oval are judged incorrectly as enriched by an asymptotical function. Because of this judgment error, the final path of the two methods is slightly different, as shown in Fig. 13. From the amplified image in Fig. 14, it is known that the different types of nodes begin in the third step, at which point the Heaviside enrichment nodes are judged incorrectly as asymptotic enrichment nodes.

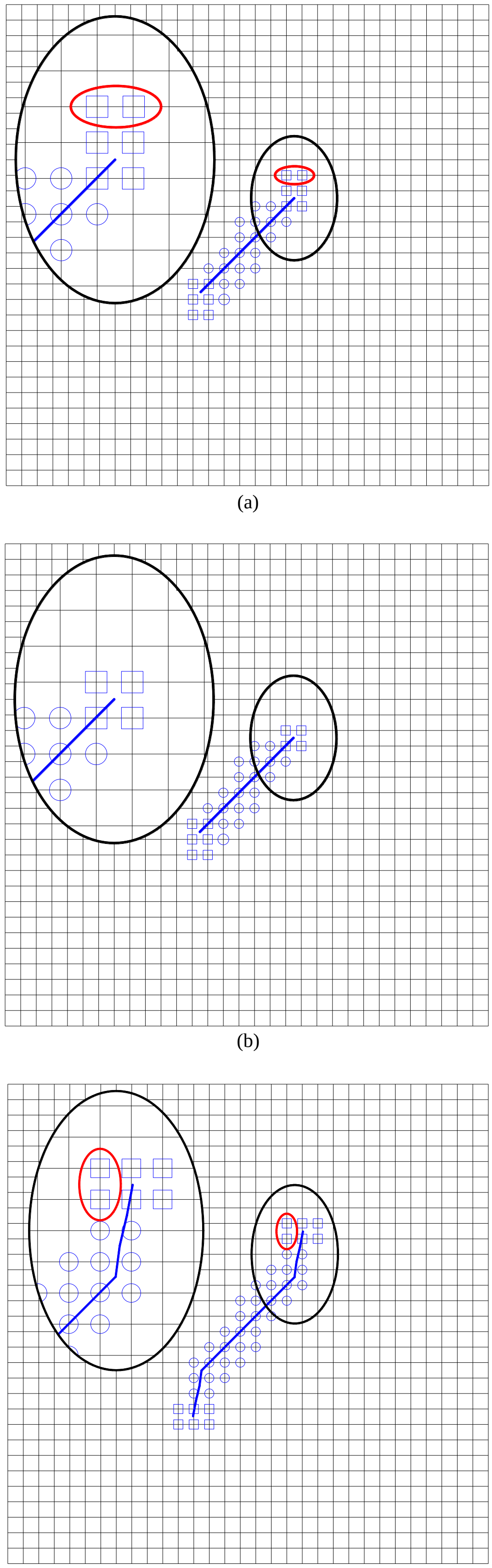

(a)

(b)

(c)

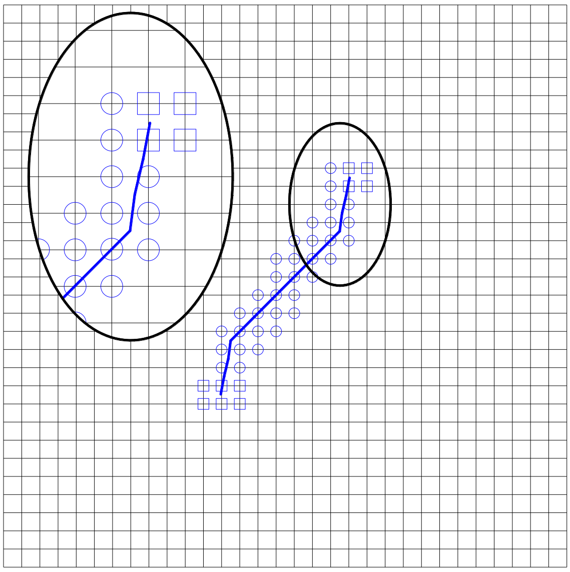

(d)

Fig. 12. Nodes enriched by two methods in different steps: (a) and (c) by LSM in the first and third steps; (b) and (d) by the proposed method in the first and third steps.

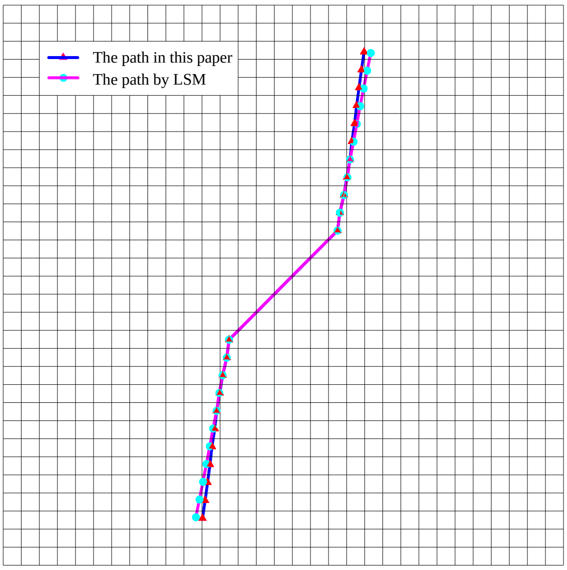

Fig. 13. Final paths of the two methods.

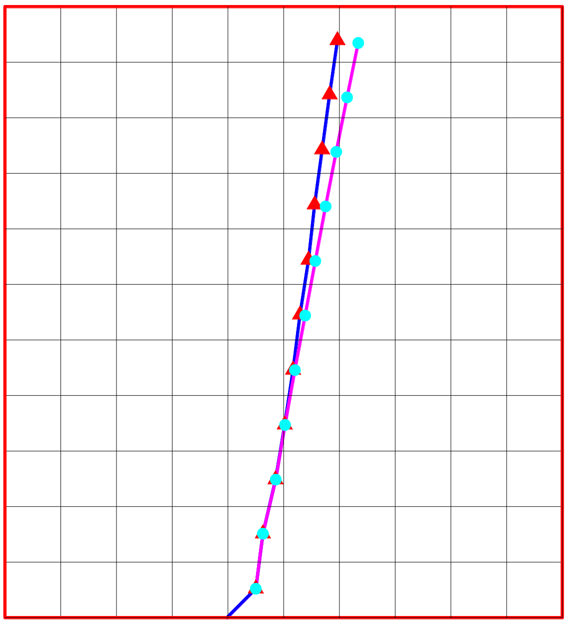

Fig. 14. Local amplified figure for final paths.

As shown in Table I, the incorrect judgment that occurs in the first step of the LSM has little effect on the SIFs. However, the SIFs calculated by the LSM are obviously lower than the factors by the method proposed in this paper because the Heaviside enrichment nodes are judged incorrectly as asymptotical nodes; that is, an error caused by the incorrect judgment for a standard node is very small, but it is obvious for the Heaviside enrichment nodes.

TABLE I
STRESS INTENSITY FACTORS IN FIRST THREE STEPS

	Method proposed in this paper		LSM	
SIF	K_I/σ_y $(m^{1/2})$	K_{II}/σ_y $(m^{1/2})$	K_I/σ_y $(m^{1/2})$	K_{II}/σ_y $(m^{1/2})$
Step 1	4.699229423	−2.077539601	4.743337507	−2.081772594
Step 2	6.681395712	0.32907408	6.665458717	0.342777216
Step 3	7.837850418	−0.250388707	7.426714655	−0.168975847

Comparison of Overall Computer Time

From the flowchart in Fig. 6, and according to the algorithm given in Section 3.2 with a simple condition sentence, the speed in the proposed method is faster than that in the LSM with strenuous computation, variable storage, and a judgment sentence. Khoei [43] indicated that it is not necessary to perform the LS computation for the entire domain because it can be calculated in the narrow bandwidth. Pais [53] achieved this algorithm using MATLAB code. Fig. 15 gives the average computation time for the two methods to run continuously 10 times under the same conditions with different element numbers in the first step of the MATLAB code. It was found that the calculation efficiency will be improved by at least 14%.

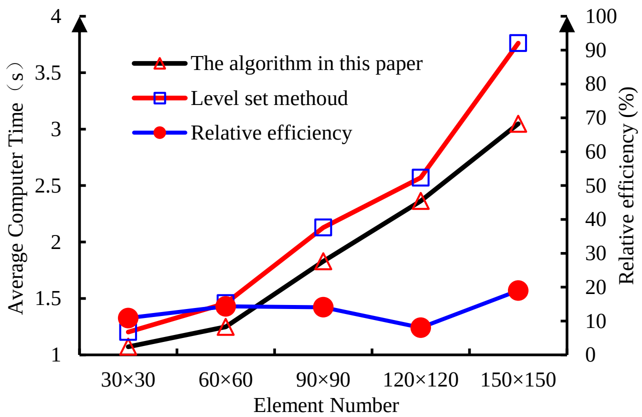

Fig. 15. Average computer time of center slant crack model in first step.

C. *Paths of Interactive Crack Growth*

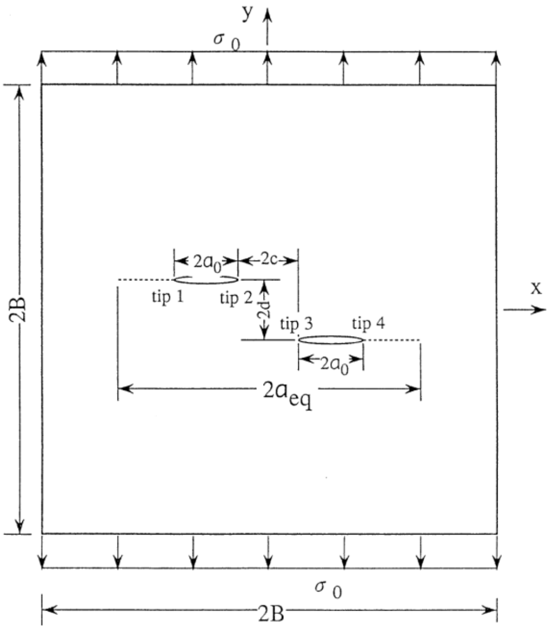

Fig. 16. Computing model of two internal interactive cracks.

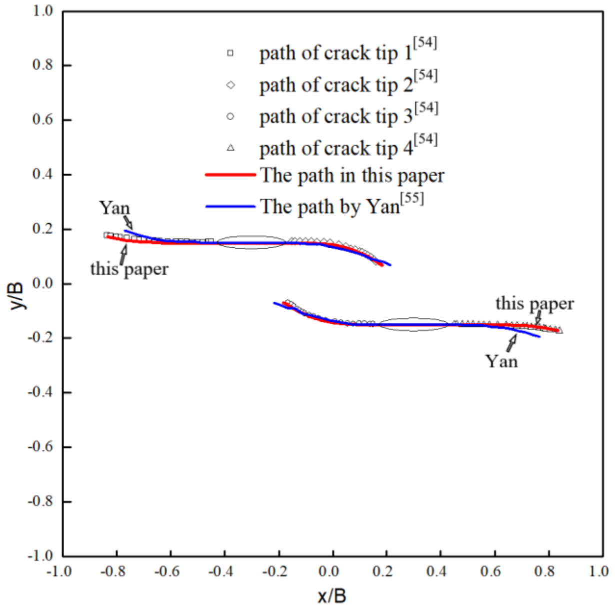

Fig. 17. Entire paths of two interactive cracks.

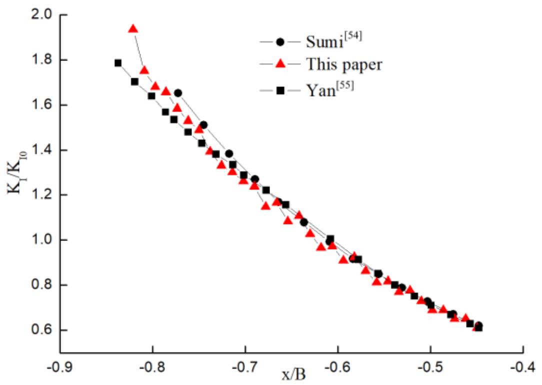

(a) Crack tip 1

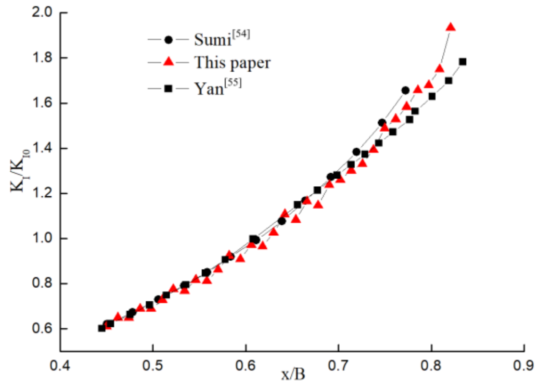

(b) Crack tip 4

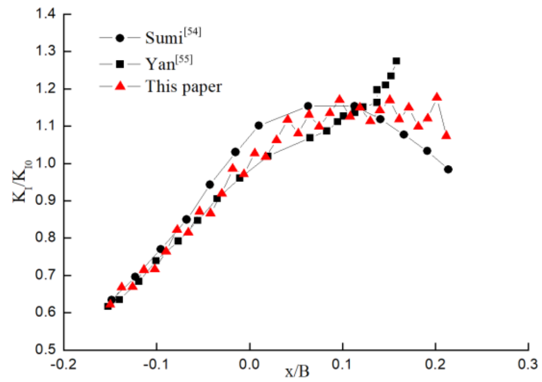

(c) Crack tip 2

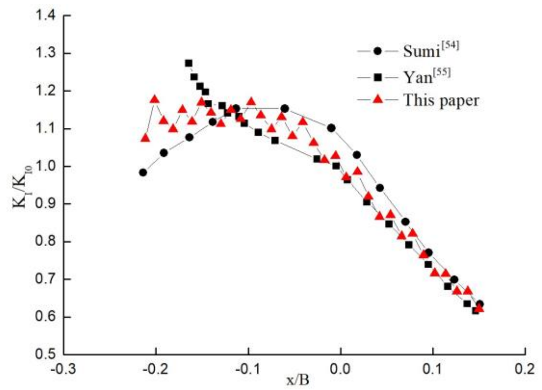

(d) Crack tip 3

Fig. 18. Non-dimensional stress intensity factors at four crack tips.

Sumi [54] simulated interactive crack growth with double internal cracks and suggested that the interaction of crack growth would occur when the crack tips closely approach each other. The computation model is shown in Fig. 16. The non-dimensional size is set by $a_0/B = 0.4$, $c/a_0 = 1.0$, and $d/a_0 = 1.0$, and the material parameters, Young's modulus and Poisson's ratio, are assumed to be 200 GPa and 0.3, respectively. The uniform tensile stress σ_0 is prescribed on the upper and lower edges of the plate. Yan [55] simulated the same model using the cellular automation method. These authors all have pointed out that the paths of the internal crack tips are curved towards the interior and the exterior crack tips are slightly curved in a clockwise direction. The proposed algorithm was used to compute the same model, and it was found that the paths of the growth crack were almost the same as those computed by Sumi [54], as shown in

Fig. 17. Fig. 18 gives the non-dimensional SIFs at the crack tips, where $K_{10} = \sigma_0 \sqrt{\pi a_{aq}}$, and the results of tips 1 and 4 are almost the same as Sumi's and Yan's. However, from Section 5.2.1, it is known that an incorrect judgment will cause the SIF to be relatively small, so that the non-dimensional SIF calculated by Yan is relatively small. The crack-tip-embedded element is semi-continuous in the XFEM, which may cause the enrichment stiffness matrix to be slightly more rigid than in the FEM, such that the crack forms a boundary so that the non-dimensional SIF calculated by Sumi is relatively large. The results of tips 2 and 3 not only depend on the SIF, but also on the length of a_{aq}. The results of this paper are nearly the average of their results but closer to Sumi's.

D. Searching the Enriched Element in Three Dimensions

Because the dimension of the crack in the 3D model is one order higher than in the 2D model, the elements that are crossed by the crack boundary are enriched by the Heaviside function, and the elements crossed by the domain of the crack are enriched by the asymptotic function. Both the inflection points of the boundary for the crack plane and the domain of the crack plane should be considered separately. The regular and irregular boundaries of the crack are used as examples and the different types of elements are given.

Regular Boundary for Crack Plane

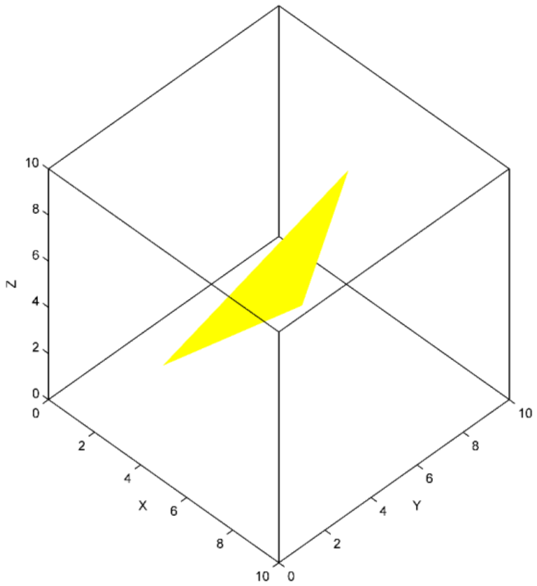

Fig. 19. Model with triangular crack plane in 3D model.

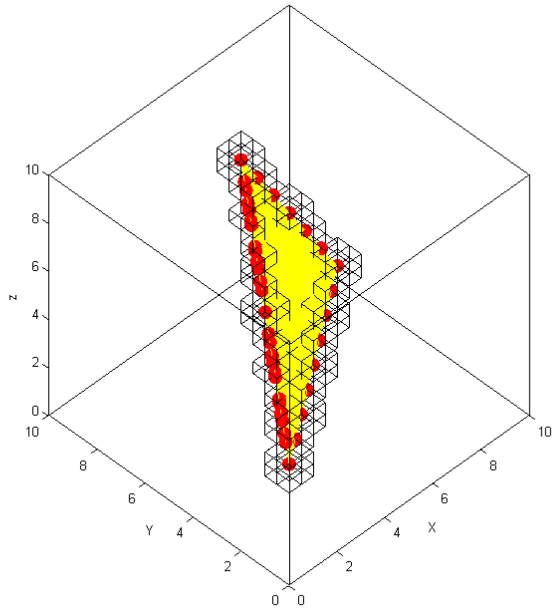

(a) Elements and intersection points embedded by crack boundary in 3D model

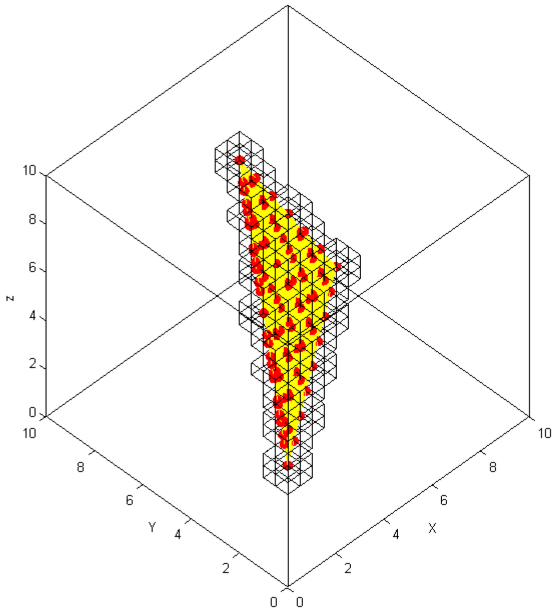

(b) Whole results

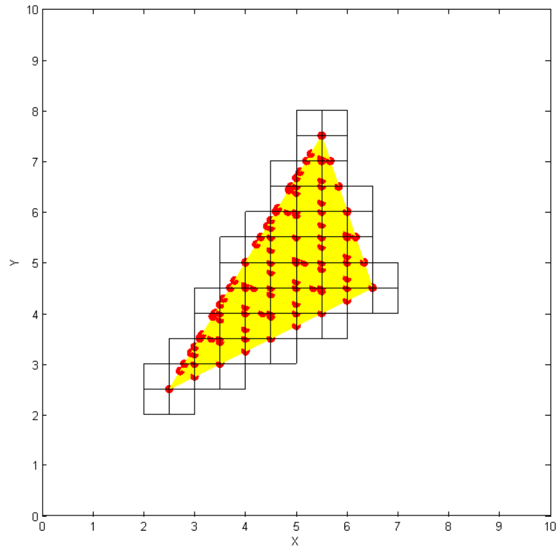

(c) Results in z direction

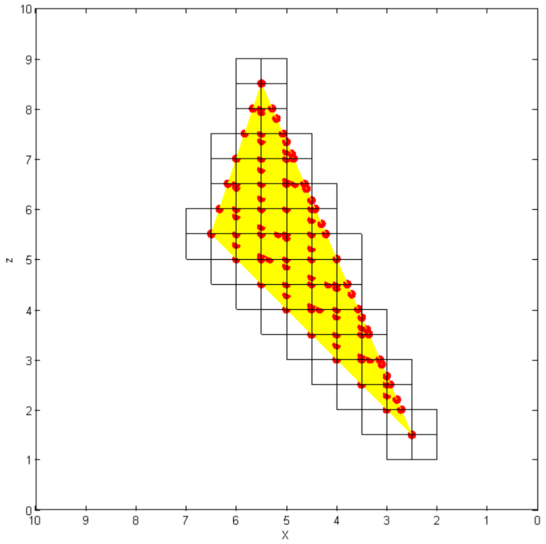

(d) Results in y direction

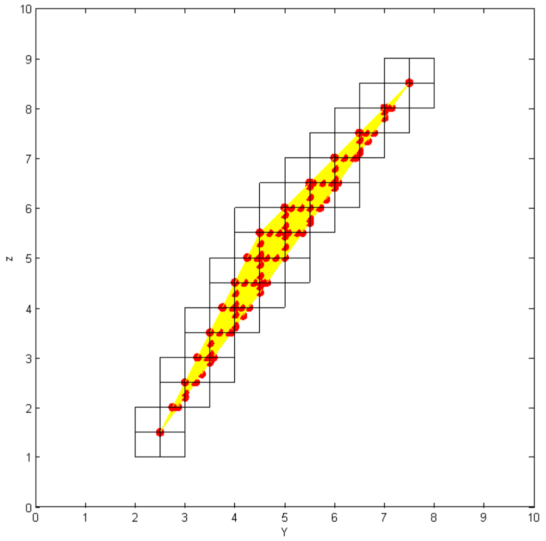

(e) Results in x direction

Fig. 20. Search results for all enriched elements and intersection points between element and crack; red circle (●) is intersection point.

Fig. 19 shows a triangular crack plane in the 3D model. The size of the model is the following: length = 10 m, width = 10 m, height = 10 m, and the crack plane is set by the points (2.5, 2.5, 1.5), (6.5, 4.5, 5.5), and (5.5, 7.5, 8.5). The mesh element number of the model is 20 × 20 × 20. The search results of the enriched elements and their types are shown in Fig. 20.

Irregular Boundary for Crack Plane

In the 3D model, the crack boundary cannot be always regular. Fig. 21 shows an elliptical plane crack as the irregular boundary; the position and the size of the crack are established by the equation set $\begin{cases} \frac{(x-5)^2}{16}+\frac{(y-5)^2}{4}=1 \\ z=\frac{\sqrt{3}}{3}(x-5)+5 \end{cases}$, and the model is a cube with a side length of 10 m and the mesh element number is 20 × 20 × 20. The different types of enrichment elements are computed in Fig. 22. The enrichment elements and key information about the intersection relationship are given for the different projection directions in Fig. 23.

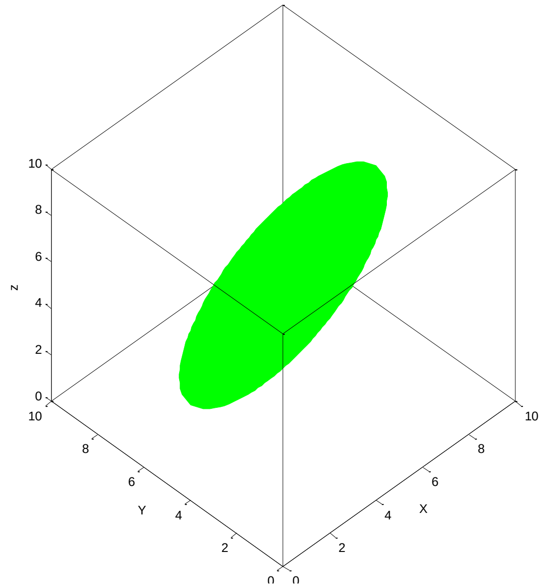

Fig. 21. Model with irregular boundary for crack plane.

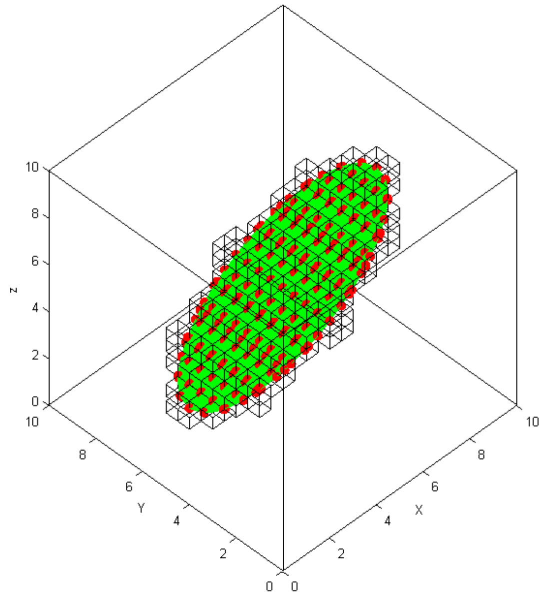

(a) Whole results

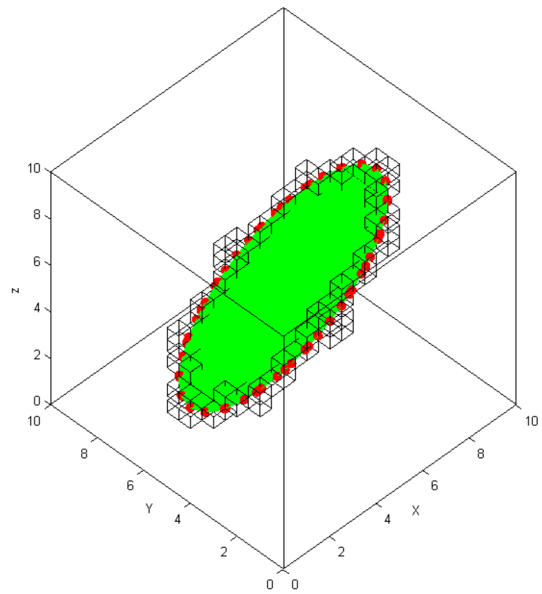

(b) Element embedded by crack boundary

Fig. 22. Search results for enriched elements and intersection points between element and crack; red circle (●) is intersection point.

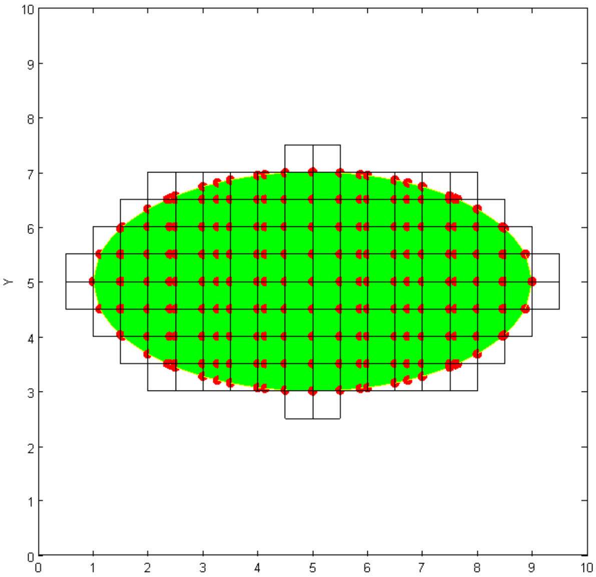
(a) Projection in z direction

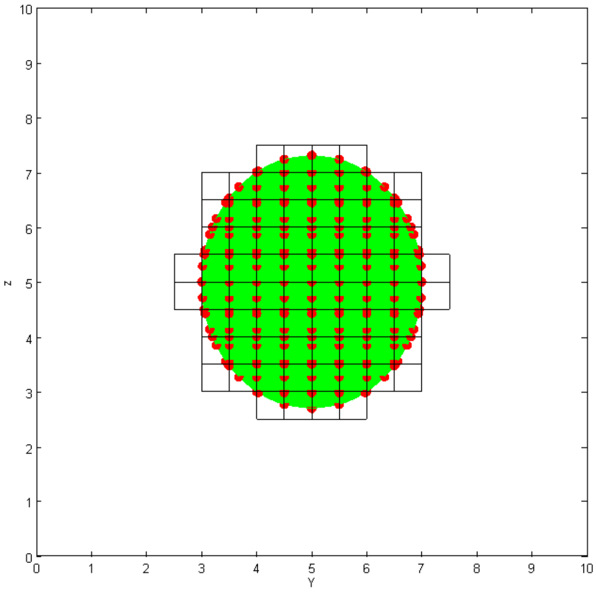
(b) Projection in x direction

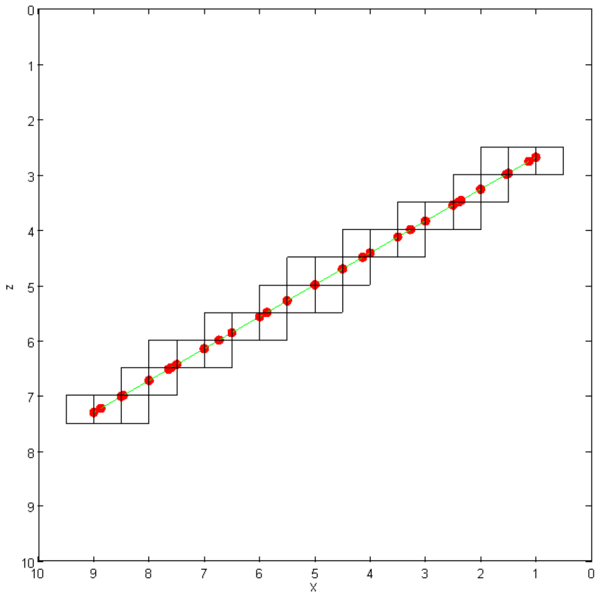
(c) Projection in y direction

Fig. 23. Results in different projection directions; ● marks intersection point.

VI. Conclusions

Structural meshing is a convenient and effective technique used in the extended finite-element method (XFEM) because the finite-element mesh is completely independent of cracks. To make full use of its advantages, an algorithm based on the positional relationship between element boundaries and cracks was proposed herein to search the enrichment elements and judge element types. Furthermore, numerical simulation was used to study the accuracy, computational efficiency, and storage consumption of the proposed algorithm, as well as to explore the extension to 3D applications. Based on these results, the following conclusions are drawn.

(1) With the proposed algorithm, not only can the information between the element boundary and the crack be obtained by computation, but the errors in judgment about the crack-tip-embedded element can be avoided.

(2) In the 2D model, the proposed MATLAB-based algorithm requires only one level set value of the enrichment nodes, i.e., the horizontal signed distance value, to be computed under the same conditions, compared to two level set values of multiple nodes that must be computed using the level set method (LSM), thereby resulting in faster computation speed on average than the LSM with a narrow bandwidth. In addition, since the cracks and boundaries of the element are 1D, the new algorithm is simpler and has lower storage consumption.

(3) In the 3D model, using the proposed algorithm, it is possible to perform the same computations in three projection directions to accurately capture critical information about the intersection of the crack surface and elemental boundaries.

Acknowledgements

This study was supported by the Strategic Program of the Chinese Academy of Sciences (Shale fracturing and multi-scale seepage in shale reservoir, Grant No. XDB10030400) and the Hundred Talent Program of the Chinese Academy of Sciences (Shale hydraulic fracturing and multi-scale seepage mechanism and model, Grant No. Y323081C01). The authors express their deepest gratitude for their generous support. The authors declare that there are no conflicts of interest regarding the publication of this paper.

References

[1] Azadi H, Khoei A, “Numerical simulation of multiple crack growth in brittle materials with adaptive remeshing,” International Journal for Numerical Methods in Engineering, vol. 85, no. 8, pp. 1017-1048, 2011.
[2] Song J, Zhou J T, Jiang R, Wang M B, Yu X, Jia S L, et al., “Fatigue Crack Propagation in BFRP Reinforced RC Beams Based on Fracture Mechanics and Golden Ratio,” Engineering Letters, vol. 24, no. 4, pp. 449-454, 2016.
[3] Zakhezin A, Pryadko Y, Kolosova O and Aliukov S, “Diagnostics of Fatigue Cracks in Rotor Systems of Machines,” Engineering Letters, vol. 28, no. 1, pp. 209-214, 2020.
[4] Blandford GE, Ingraffea AR, Liggett JA. “Two-dimensional stress intensity factor computations using the boundary element method,” International Journal for Numerical Methods in Engineering, vol. 17, no. 3, pp. 387-404, 1981.

[5] Deng S, Li H, Ma G, Huang H and Li X, “Simulation of shale–proppant interaction in hydraulic fracturing by the discrete element method,” Int J Rock Mech Min, vol. 70, pp. 219-228, 2014.

[6] Belytschko T, Gu L and Lu Y, “Fracture and crack growth by element free Galerkin methods,” Model Simul Mater Sc, vol. 2, no. 3A, pp. 519-534, 1994.

[7] Belytschko T, Black T, “Elastic crack growth in finite elements with minimal remeshing,” International Journal for Numerical Methods in Engineering, vol. 45, no. 5, pp. 601-620, 1999.

[8] Budyn E, Zi G, Moes N and Belytschko T. “A method for multiple crack growth in brittle materials without remeshing,” International Journal for Numerical Methods in Engineering, vol. 61, no. 10, pp. 1741-1770, 2004.

[9] Dahi Taleghani A, “Analysis of hydraulic fracture propagation in fractured reservoirs: an improved model for the interaction between induced and natural fractures,” The University of Texas at Austin, May 2009.

[10] Sukumar N, Chopp DL, Moes N and Belytschko T, “Modeling holes and inclusions by level sets in the extended finite-element method,” Computer Methods in Applied Mechanics and Engineering, vol. 190, no.46-47, pp. 6183-6200, 2001.

[11] Dolbow J, Moes N and Belytschko T, “An extended finite element method for modeling crack growth with frictional contact,” Computer Methods in Applied Mechanics and Engineering, vol. 190, no. 51-52, pp. 6825-6846, 2001.

[12] Khoei AR, Shamloo A and Azami AR, “Extended finite element method in plasticity forming of powder compaction with contact friction,” Int J Solids Struct, vol. 43, no. 18-19, pp. 5421-5448, 2006.

[13] Khoei AR, Anahid M, Yadegaran I and Nikbakht M, “Implementation of the eXtended Finite Element Method (X-FEM) in frictional contact problems,” NUMIFORM '07: Materials Processing and Design: Modeling, Simulation and Applications, Pts I and II, vol. 908, pp. 1573-1578, 2007.

[14] Ventura G, Budyn E and Belytschko T, “Vector level sets for description of propagating cracks in finite elements,” International Journal for Numerical Methods in Engineering, vol. 58, no. 10, pp. 1571-1592, 2003.

[15] Gravouil A, Moës N and Belytschko T, “Non-planar 3D crack growth by the extended finite element and level sets—Part II: Level set update,” International Journal for Numerical Methods in Engineering, vol. 53, no. 11, pp. 2569-2586, 2002.

[16] Moës N, Gravouil A and Belytschko T, “Non-planar 3D crack growth by the extended finite element and level sets—Part I: Mechanical model,” International Journal for Numerical Methods in Engineering, vol. 53, no. 11, pp. 2549-2568, 2002.

[17] Stolarska M, Chopp DL, Moes N and Belytschko T, “Modelling crack growth by level sets in the extended finite element method,” International Journal for Numerical Methods in Engineering, vol. 51, no. 8, pp. 943-960, 2001.

[18] Sukumar N, Chopp D, Béchet E and Moës N, “Three-dimensional non-planar crack growth by a coupled extended finite element and fast marching method,” International Journal for Numerical Methods in Engineering, vol. 76, no. 5, pp. 727-748, 2008.

[19] Chopp DL, Sukumar N, “Fatigue crack propagation of multiple coplanar cracks with the coupled extended finite element/fast marching method,” Int J Eng Sci, vol. 41, no. 8, pp. 845-869, 2003.

[20] Wagner G, Moës N, Liu W and Belytschko T, “The extended finite element method for rigid particles in Stokes flow,” International Journal for Numerical Methods in Engineering, vol. 51, no. 3, pp. 293-313, 2001.

[21] Gerstenberger A, Wall WA, “An extended finite element method/Lagrange multiplier based approach for fluid–structure interaction,” Computer Methods in Applied Mechanics and Engineering, vol. 197, no. 19, pp. 1699-1714, 2008.

[22] Dolbow J, Mosso S, Robbins J and Voth T, “Coupling volume-of-fluid based interface reconstructions with the extended finite element method,” Computer Methods in Applied Mechanics and Engineering, vol. 197, no. 5, pp. 439-447, 2008.

[23] Shi F, Wang XL, Liu C, Liu H and Wu HA, “A coupled extended finite element approach for modeling hydraulic fracturing in consideration of proppant,” J Nat Gas Sci Eng, vol. 33, pp. 885-897, 2016.

[24] Mohammadnejad T, Khoei AR, “Hydro-Mechanical Modeling of Two-Phase Fluid Flow in Deforming, Partially Saturated Porous Media with Propagating Cohesive Cracks Using the Extended Finite Element Method,” Computational Plasticity Xi: Fundamentals and Applications, pp. 1527-1538, 2011.

[25] Kamran K, Rossi R and Onate E, “A locally extended finite element method for the simulation of multi-fluid flows using the Particle Level Set method,” Computer Methods in Applied Mechanics and Engineering, vol. 294, pp. 1-18, 2015.

[26] Khoei AR, Hosseini N and Mohammadnejad T, “Numerical modeling of two-phase fluid flow in deformable fractured porous media using the extended finite element method and an equivalent continuum model,” Adv Water Resour, vol. 94, pp. 510-528, 2016.

[27] Liu PL, Liu F, She CY, Zhao LQ, Luo ZF, Guan WT, et al., “Multi-phase fracturing fluid leakoff model for fractured reservoir using extended finite element method,” J Nat Gas Sci Eng, vol. 28, pp. 548-557, 2016.

[28] Ren QW, Dong YW and Yu TT, “Numerical modeling of concrete hydraulic fracturing with extended finite element method,” Sci China Ser E, vol. 52, no. 3, pp. 559-565, 2009.

[29] Mohammadnejad T, Khoei AR, “An extended finite element method for hydraulic fracture propagation in deformable porous media with the cohesive crack model,” Finite Elem Anal Des, vol. 73, pp. 77-95, 2013.

[30] Wang DX, Zhou B and Xue SF, “Simulation on hydraulic fracturing propagation using extended finite element method,” Advances in Energy, Environment and Materials Science, pp. 455-458, 2016.

[31] Moës, JD, TB, “A finite element method for crack growth without remeshing,” International Journal for Numerical Methods in Engineering, vol. 46, no. 1, pp. 131-150, 1999.

[32] Osher S, Sethian JA, “Fronts propagating with curvature-dependent speed: algorithms based on Hamilton-Jacobi formulations,” J Comput Phys, vol. 79, no. 1, pp. 12-49, 1988.

[33] Filipovic L, Selberherr S, Mutinati G C, Brunet E, Steinhauer S, Köck A, et al., “A method for simulating spray pyrolysis deposition in the level set framework,” Engineering Letters, vol. 21, no. 4, pp. 224-240, 2013.

[34] Sethian JA, Level set methods and fast marching methods: evolving interfaces in computational geometry, fluid mechanics, computer vision, and materials science (Book style), Cambridge University Press, 1999.

[35] Zhuang Z. Extended finite element method (Book style), First edition.

[36] Osher S, Fedkiw R, Level set methods and dynamic implicit surfaces (Book style), Springer Science & Business Media, 2006.

[37] Sethian JA, “Level set methods and fast marching methods,” Journal of Computing and Information Technology, vol. 11, no. 1, pp. 1-2, 2003.

[38] Khoei, Amir R, Extended finite element method: theory and applications (Book style), John Wiley & Sons, 2014.

[39] Adalsteinsson D, Sethian JA, “A Fast Level Set Method for Propagating Interfaces,” J Comput Phys, vol. 118, no. 2, pp. 269-277, 1995.

[40] Sethian JA, “A fast marching level set method for monotonically advancing fronts,” P Natl Acad Sci USA, vol. 93, no. 4, pp. 1591-1595, 1996.

[41] Forcadel N, “Generalized Fast Marching Method and Applications”, University Paris Dauphine, 2011.

[42] Mohammadi S, Extended finite element method for fracture analysis of structures (Book style), Oxford; Malden, MA: Blackwell Pub, 2008.

[43] Khoei AR, Extended finite element method: theory and applications (Book style), John Wiley & Sons, 2014

[44] Chopp DL, “Some improvements of the fast marching method,” Siam J Sci Comput, vol. 23, no. 1, pp. 230-244, 2001.

[45] Sukumar N, Chopp D and Moran B, “Extended finite element method and fast marching method for three-dimensional fatigue crack propagation,” Eng Fract Mech, vol. 70, no. 1, pp. 29-48, 2003.

[46] Sukumar N, Chopp DL, Bechet E and Moes N, “Three-dimensional non-planar crack growth by a coupled extended finite element and fast marching method,” International Journal for Numerical Methods in Engineering, vol. 76, no. 5, pp. 727-748, 2008.

[47] Dolbow JE, “An extended finite element method with discontinuous enrichment for applied mechanics,” Northwestern University, 1999.

[48] Daux C, Moes N, Dolbow J, Sukumar N and Belytschko T, “Arbitrary branched and intersecting cracks with the extended finite element method,” International Journal for Numerical Methods in Engineering, vol. 48, no. 12, pp. 1741-1760, 2000.

[49] Belytschko T, Parimi C, Moes N, Sukumar N and Usui S, “Structured extended finite element methods for solids defined by implicit surfaces,” International Journal for Numerical Methods in Engineering, vol. 56, no. 4, pp. 609-635, 2003.

[50] Belytschko T, Moës N, Usui S and Parimi C, “Arbitrary discontinuities in finite elements,” International Journal for Numerical Methods in Engineering, vol. 50, no. 4, pp. 993-1013, 2001.

[51] Sih G, Paris P and Erdogan F, “Crack-tip, stress-intensity factors for plane extension and plate bending problems,” Journal of Applied Mechanics, vol. 29, no. 2, pp. 306-312, 1962.

[52] Erdogan F, Sih G, “On the crack extension in plates under plane loading and transverse shear,” Journal of Basic Engineering, vol. 85, no. 4, pp. 519-527, 1963.

[53] Pais M. Matlab extended finite element (MXFEM) code v1. 2. 2011.
[54] Sumi Y, Wang Z, “A finite-element simulation method for a system of growing cracks in a heterogeneous material,” Mech Mater, vol. 28, no. 1, pp. 197-206, 1998.
[55] Yan F, Feng XT, Pan PZ and Li SJ, “Discontinuous cellular automaton method for crack growth analysis without remeshing,” Appl Math Model, vol. 38, no. 1, pp. 291-307, 2014.